would be required to reconcile the present ΔV_m^{eff} with a $0.7V_a$ value for ΔV_m^v. There is little, if any, experimental evidence to support a lower value for E_b^{vv}. Admittedly, the frequency factors used in the calculation have not been verified and some of the other measured quantities are uncertain. Nonetheless, such a large single-vacancy ΔV_m should be evident in our low-temperature quench measurements.

The value of ΔV_{sd} for aluminum is larger than for other metals studied to date, whose values range from 0.7 to $0.9V_a$.[3,28] A possible reason for the large ΔV_{sd} in aluminum is that there is a divacancy contribution to self-diffusion. This conclusion is supported by the measured increase of E_{sd} with increasing temperature,[29] although Stoebe and Dawson argue that divacancies alone cannot explain the entire temperature dependence. Another possibility is a temperature dependence of ΔV_m. Both ΔV_{sd} and ΔV_f^v are measured near the melting point, whereas ΔV_m has been measured at room temperature and below. This is also consistent with Stoebe and Dawson's conclusions that there is a temperature dependence of E_m^v. Enough data are not yet available to decide the relative importance of these contributions in the present case.

[28] Y. Adda and J. Philibert, *La Diffusion dans les Solides* (Presses Universitaires de France, Paris, 1966), Vol. II.
[29] T. G. Stoebe and H. I. Dawson, Phys. Rev. 166, 621 (1968).

V. SUMMARY

The pressure effect on the annealing of electrical resistance quenched into aluminum from two different temperatures was studied. The effective motional volumes were $(0.17\pm0.02)V_a$ for quenches from 580°C and $(0.18\pm0.02)V_a$ for quenches from 331°C. The former is attributed to divacancies. The latter should show evidence of a single-vacancy contribution. It is consistent with these and other pressure data for aluminum that the single-vacancy motional volume is not appreciably different from this value and that the large self-diffusion activation volume in aluminum is the result of a divacancy contribution to diffusion or a temperature dependence of ΔV_m.

PHYSICAL REVIEW B VOLUME 1, NUMBER 10 15 MAY 1970

Landau Quantum Oscillations of the Velocity of Sound in Be: The Strain Dependence of the Fermi Surface

L. R. TESTARDI AND J. H. CONDON
Bell Telephone Laboratories, Murray Hill, New Jersey 07974
(Received 4 November 1969)

Landau quantum oscillations of the velocity of sound in Be are reported. A general thermodynamic relation between the quantum oscillations of the velocity of sound (elastic moduli) and the strain dependence of the Fermi surface is given and is used to interpret the results. This relation shows that the amplitude of the oscillations is determined by the magnetic susceptibility and the strain dependence of the Fermi-surface extremal areas. An oscillatory as well as a monotonic Alpher-Rubin effect is obtained in this treatment. All major features of this theoretical result are generally verified in the experimental results. The strain dependence of the Fermi surface obtained in this work is in susbtantial agreement with previous hydrostatic pressure studies. At low temperatures, magnetic interaction effects modily the oscillation pattern. These results imply that the (differential) susceptibility at high frequencies is never paramagnetic. This behavior is shown to be consistent with the presence of magnetic domains whose walls are immobile at the sound frequency. Experimental techniques are also presented.

I. INTRODUCTION

IN recent years, Landau quantum oscillations in the velocity of sound have been reported in Bi,[1] Au,[2] and Ga.[3] To date, much of the information provided by these experiments has been limited to determinations, from the measured periods, of the extremal areas of the Fermi surface.[4] Although the conditions normally necessary for the occurrence of Landau quantum oscillations ($\omega_c\tau>1$ and $\hbar\omega_c>kT$) apply as well to the sound velocity behavior, it is apparent on physical grounds that in the latter case the amplitude of the oscillations must also reflect the deformation properties of the Fermi surface. Attempts to calculate the amplitude of this effect[5–7] in terms of all controlling factors are generally compromised by simplifying assumptions in which real metal effects are precluded. There remains,

[1] J. G. Mavroides, B. Lax, K. J. Button, and Y. Shapira, Phys. Rev. Letters 9, 451 (1962).
[2] G. A. Alers and R. T. Swim, Phys. Rev. Letters 11, 72 (1963).
[3] L. J. Neuringer and Y. Shapira, Phys. Rev. 165, 751 (1968).
[4] L. J. Neuringer and Y. Shapira (Ref. 3) have applied several existing theories to account for the amplitude of the oscillations. One such theory was shown to be reasonably consistent in relating the velocity and attenuation changes.
[5] J. J. Quinn and S. Rodgriuez, Phys. Rev. Letters 9, 145, (1962).
[6] S. Rodriguez, Phys. Rev. 132, 535 (1963).
[7] A. Ya. Blank and E. A. Kaner, Zh. Eksperim. i Teor. Fiz. 50, 1013 (1966) [Soviet Phys. JETP 23, 673 (1966)].

however, a simple solution of a quite general nature which yields the direct relation between the sound velocity oscillations and the strain dependence of the Fermi surface. This procedure, which we present for the first time,[8] employs a thermodynamic argument to separate the strain dependence of the Fermi surface from all other factors which determine the amplitude. The latter part is shown to be simply the differential magnetic susceptibility dI/dB which we obtain by separate measurement. This treatment, described in Sec. II, also shows a simple thermodynamic derivation of the Alpher-Rubin effect.[9] For longitudinal waves propagating normal to the applied field, the Alpher-Rubin effect is shown to give an additional oscillatory contribution to the sound velocity. This treatment, which is quite general, allows the complete (longitudinal as well as shear) strain dependence of the Fermi surface to be obtained from sound velocity measurements.

For Be the oscillatory magnetization from part of the Fermi surface becomes so large that nonlinear magnetic interaction (MI) effects occur.[10,11] For large MI effects, magnetic domain formation has been predicted.[12] Our treatment of the sound velocity oscillations is extended to such cases and ultimately yields information on these effects at high frequencies.

In Sec. III we describe our methods to measure the absolute values of the magnetization and its derivatives, dI/dH and dI/dB, versus H or B for samples of unknown demagnetizing factor. The results of the magnetization measurements are given in Sec. IV.

To obtain continuous recording of high precision sound velocity data, we have used an FM modification of the McSkimin pulse superposition method[13] to provide automatic frequency control. The arrangement is described in some detail in Sec. V. Section VI covers the results of sound velocity measurements and the strain dependence of the Fermi surface so obtained. A discussion of the sound velocity in the region of large MI effects is also given. A comparison of our results wlth existing data is made in Sec. VII.

II. THEORY

The elastic moduli of a material are the second derivatives of a thermodynamic potential with respect to strain,[14]

$$c=d^2U/d\epsilon^2. \tag{1}$$

This same potential function should also describe the magnetic behavior of the material. Since the function

$$U=\tfrac{1}{2}\boldsymbol{\varepsilon}\cdot\mathbf{c}_l\cdot\boldsymbol{\varepsilon}+\Omega(\mathbf{B},\epsilon)+B^2/8\pi \tag{2}$$

has the property

$$\left.\frac{\partial U}{\partial \mathbf{B}}\right|_{\epsilon}=\mathbf{H}/4\pi, \tag{3}$$

which is easily relatable to the usual definition of the magnetic free energy, we shall treat U as the correct free energy. $\mathbf{c}_l$ is the background elastic modulus and includes the lattice stiffness and any nonoscillatory electron-gas stiffness. $\Omega(\mathbf{B},\boldsymbol{\varepsilon})$ is the oscillatory electronic free energy similar to that given by Lifshitz and Kosevich[15] but suitably modified to include impurity scattering, inhomogeneity broadening, magnetic breakdown, and any other effect that might modify the amplitude of the Landau oscillatory effects. The magnetization is given by $\mathbf{I}=-\partial\Omega/\partial\mathbf{B}|_{\epsilon}$.

Because of the nature of the function Ω, its derivatives with respect to strain can be related to those with respect to the magnetic induction B. The function Ω is a rapidly oscillating function of the form

$$\Omega=C(\mathbf{B},\boldsymbol{\varepsilon})\cos[A(\boldsymbol{\varepsilon})/B], \tag{4}$$

where C is a slow amplitude function, and A is the strain-dependent extremal Fermi-surface cross-sectional area. Since the predominant derivatives come from the cosine term, the strain and induction derivatives are related by

$$\partial/\partial\boldsymbol{\varepsilon}\cong -B\mathbf{D}(\partial/\partial B), \tag{5}$$

where the "deformation parameter" $\mathbf{D}$ is a tensor like $\boldsymbol{\varepsilon}$, whose 1×6 matrix components are

$$D_i\equiv(\partial/\partial\epsilon_i)\ln A(\epsilon). \tag{6}$$

At frequencies such that the sound wavelength λ is small compared to the sample size,[16] but large compared to the classical skin depth,[17] the strain and magnetic induction are interdependent. Eddy currents exist in the material such that the lines of B move with the particle

[8] T. Thompson (private communication) has also used thermodynamic arguments in a similar calculation. His results do not include the oscillatory Alpher-Rubin effect (see below).

[9] The Alpher-Rubin effect is the increase in sound velocity of a metal when in a magnetic field. R. A. Alpher and R. J. Rubin, J. Acoust. Soc. Am. **26**, 452 (1954).

[10] D. Shoenberg, Phil. Trans. Roy. Soc. London **A255**, 85 (1962).

[11] A. B. Pippard, Proc. Roy. Soc. (London) **A272**, 192 (1963).

[12] J. H. Condon, Phys. Rev. **145**, 526 (1966).

[13] H. J. McSkimin, J. Acoust. Soc. Am. **33**, 12 (1961).

[14] In the derivation to follow all derivatives are taken at constant temperature. The quantity $(d^2F/d\epsilon^2)_T$, then, defines the isothermal elastic moduli. At low temperatures the thermal diffusion time over a sound wavelength is less than the sound period ω^{-1} ($\omega=2\pi\times20$ MHz). No temperature gradients occur in this case and the sound velocity is determined by the isothermal (rather than adiabatic) elastic moduli.

[15] I. M. Lifshitz and A. M. Kosivich, Zh. Eksperim. i Teor. Fiz. **29**, 730 (1955) [Soviet Phys. JETP **2**, 636 (1956)].

[16] In what follows it is assumed that the demagnetizing factor of the sound wave pattern is small. This at least requires that the sample be large compared to λ. This condition is normally met in most experiments.

[17] The requirement (for effective shielding) that the classical skin depth δ, of the eddy current fields be much less than a wavelength is well met in Be; $\delta/\lambda\sim10^{-2}$.

motion of the material; stated more precisely, because of the conductivity of the material the total flux through *any* loop which is fixed everywhere to move with the particle motion is a constant. Because of the coupling between induction and strain the "total" operator, required by Eq. (1), is given by

$$\frac{d}{d\epsilon}=\frac{\partial}{\partial\epsilon}\bigg|_B+\frac{d\mathbf{B}}{d\epsilon}\frac{\partial}{\partial\mathbf{B}}\bigg|_\epsilon. \tag{7}$$

The coupling $d\mathbf{B}/d\epsilon$ depends upon the mode of sound propagation and its direction relative to the magnetic field. For longitudinal (compressional) waves propagating perpendicularly to the induction direction the field is trapped such that an expansion ϵ decreases the local induction,

$$B=\bar{B}(1-\epsilon),\quad dB/d\epsilon=-\bar{B},\quad \text{for}\quad \mathbf{q}_L\perp\mathbf{B}. \tag{8}$$

($\bar{B}$ is the average of B over one wavelength.) For a shear (transverse) wave propagating parallel to B, the direction of B is tilted slightly from its average direction,

$$dB_p/d\epsilon=+\bar{B},\quad \text{for}\quad \mathbf{q}_T\|\mathbf{B}. \tag{9}$$

(The subscript p means the component in the particle motion direction.)

For longitudinal waves along the field direction and for shear waves propagating normal to the field there is no induction-strain coupling:

$$d\mathbf{B}/d\epsilon=0,\quad \text{for}\quad \mathbf{q}_L\|\mathbf{B}\quad\text{and}\quad \mathbf{q}_T\perp\mathbf{B}. \tag{10}$$

We now have all the relations necessary to evaluate Eq. (1) and we obtain[18,19]

$$\begin{aligned}c&=c_l-B^2D^2(dI/dB)-2B^2D(dI/dB)\\&\quad-B^2(dI/dB)+(B^2/4\pi)\\&=c_l-B^2(D+1)^2(dI/dB)+(B^2/4\pi),\quad\text{for}\quad \mathbf{q}_L\perp\mathbf{B}\end{aligned} \tag{11}$$

$$\begin{aligned}c&=c_l-B^2D^2(dI/dB)+2B^2D(dI_p/dB)\\&\quad-B^2(dI_p/dB_p)+B^2/4\pi,\quad\text{for}\quad \mathbf{q}_T\|\mathbf{B}\end{aligned} \tag{12}$$

$$c=c_l-B^2D^2(dI/dB),\quad\text{for}\quad \mathbf{q}_L\|\mathbf{B}\quad\text{and}\quad \mathbf{q}_T\perp\mathbf{B}. \tag{13}$$

The terms $c_l-B^2D^2dI/dB$ give the elastic moduli in the absence of the eddy current coupling between induction and strain. The terms $B^2(1/4\pi-dI/dB)=B^2/4\pi\mu$ in Eqs. (11) and (12) have been obtained (in a slightly different form) by Alpher and Rubin.[9]

Finally, the term $2B^2D\ dI/dB$ represents an effect which apparently has not been noted previously. The effect is an interaction between the strain-dependent magnetization of the material and the strain-dependent induction due to eddy currents. This effect will also occur in other systems, e.g., ferromagnetism, and is not unique to Landau quantum oscillatory systems.

[18] This derivation assumes $c-c_l\ll c$. If this condition is violated nonlinear elastic effects would occur.

[19] We have set $\bar{B}=B$ in Eqs. (11)–(13).

The elastic moduli are related to the sound velocity V_s and the mass density ρ by

$$\mathbf{c}=\rho V_s^2(\boldsymbol{\epsilon}). \tag{14}$$

For sound waves with strain ϵ_i, the amplitude of the quantum oscillations of V_s yields the component D_i of the deformation matrix for the corresponding Fermi surface area.

Effect of Magnetic Domains

In certain materials (Be is one) the differential susceptibility due to the de Haas–van Alphen magnetization becomes so large at low temperatures that the system can lower its free energy by breaking up into magnetic domains.[12] The domains are regions of nearly uniform magnetic induction and magnetization which are wide relative to the walls separating them.[20]

Figure 1 shows the energy function Ω and its derivatives $I=-\partial\Omega/\partial B$ and $\partial I/\partial B$ for $\sim1\frac{1}{2}$ cycles of the de Haas–van Alphen period. The solid line shows the behavior of the system if magnetic domains do not exist and the dashed line shows the behavior during the domain state. The domain state is at constant magnetic field intensity H and the change of average magnetization of the sample occurs by changing the relative size and populations of the oppositely magnetized domains. On a microscopic scale the state inside of either type of domain is described by the respective end point of the dashed lines.

The thermodynamic treatment of the elastic moduli given above is still correct when domains form; however, the susceptibility (at the 20-MHz sound frequency) will also be determined by the ability of domain walls to follow the sound stress. If the domain wall can follow the sound wave, Eqs. (11)–(13) will still be correct with $dI/dB=1/4\pi$ during the paramagnetic phase [dashed lines in Fig. 1(c)]. If the domain walls cannot move then each domain will respond to the stress according to its local state [dotted line in Fig. 1(c)]. For $|d4\pi I/dB|_{\max}>\frac{1}{2}\pi$ the domains which form during the paramagnetic phase have diamagnetic susceptibilities.[21] In this case the oscillations in the sound velocity arise only from a change in diamagnetic susceptibility between the maximum value and that value at which domains form. For these oscillations, c is always greater than c_l and no softening below the baseline will occur.

It remains to be shown whether domain wall motion will occur at 20 MHz. The major damping of wall motion should come from eddy currents. A calculation of the eddy current damping in the analogous case of ferromagnetic domains[22] shows the relaxation frequency

[20] J. H. Condon, in *Proceedings of the Tenth International Conference on Low Temperature Physics* (VINITI, Moscow, 1967), Vol. 3, p. 289.

[21] Throughout this article "diamagnetic" and "paramagnetic" will refer to the differential susceptibility dI/dB.

[22] W. P. Mason, Phys. Rev. **83**, 683 (1951).

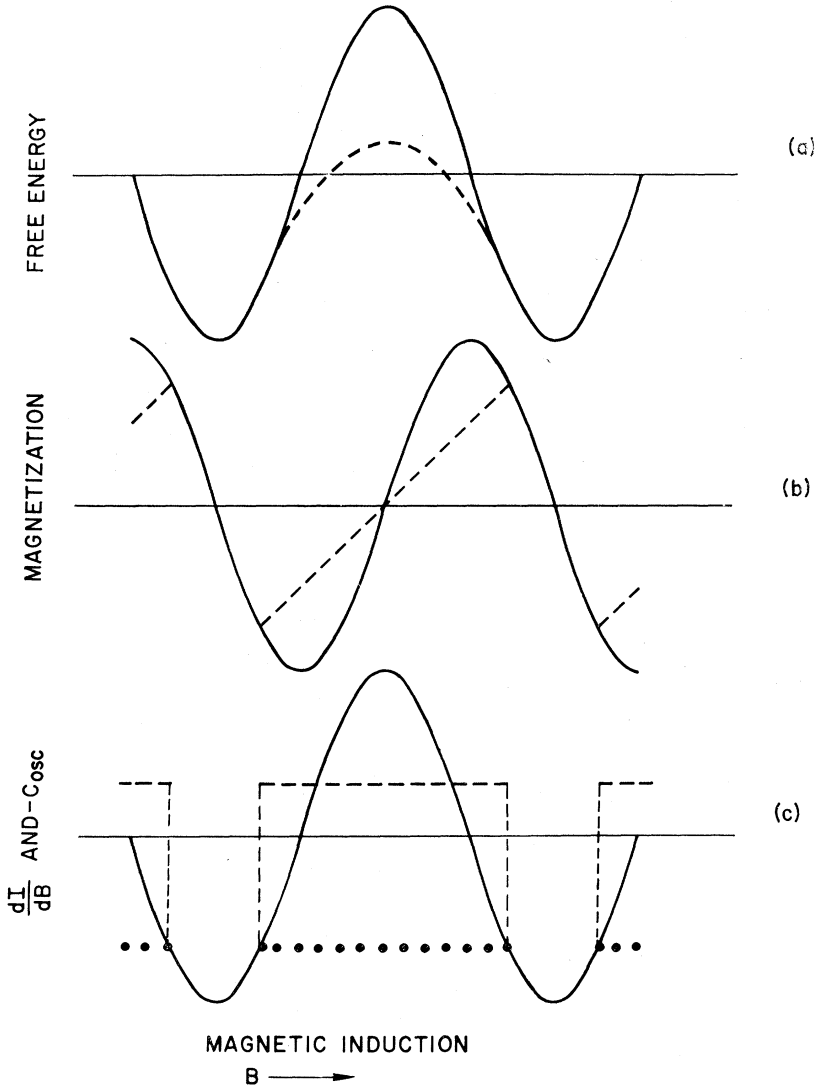

FIG. 1. (a) Free energy, (b) magnetization, (c) differential susceptibility dI/dB (or oscillatory elastic moduli) versus B. The dashed line shows the behavior for the domain state under equilibrium condition. For nonequilibrium conditions (frequencies too high for domain wall motion) the susceptibility is given by the dotted line. (The figures have been drawn for $|d4\pi I/dB|_{\max}=3.14$.)

of the motion is $\sim$100 kHz. A simple physical argument yields the same result. If the magnetic fields due to the eddy currents that are induced by domain wall motion are localized at the walls by the classical skin effect, wall motion damping will occur. If the classical skin depth is large compared to the distance between walls, the retarding fields from adjacent walls tend to cancel and the damping is reduced. The relaxation frequency for domain wall motion, then, is that frequency whose skin depth is the thickness of a domain. Condon[20] has calculated the domain thickness to be $\sim 100\,\mu$ ($H=20$ kOe, $T=1.4$°K) for which the skin depth frequency $\omega\sim c^2/2\pi l^2\sigma\approx 10^5$ Hz. We conclude, therefore, that domain wall motion will not occur at 20 MHz.

III. MAGNETIZATION MEASUREMENTS

Two methods were used to obtain absolute measurements of I, dI/dH, and dI/dB versus H or B. In Fig. 2, we show schematically the experimental arrangements used in both systems.

In one method, which measures dI/dB directly, a single layer coil (the sample coil) was wound closely on to the surface of the sample so that the current path in it closely approximated the path of the Amperian surface currents which are equivalent to the sample magnetization. By properly adjusting the current of the sample coil, it could be made to cancel the induction fields due to the magnetization both inside and outside the sample.

The sample coil current was controlled by the feedback loop shown in Fig. 2, which picked up the error signal due to the difference between sample coil field and sample magnetization field and kept it near null by adjusting the sample coil current. The induction field inside the sample was therefore equal to the applied field intensity and the current through the sample coil,

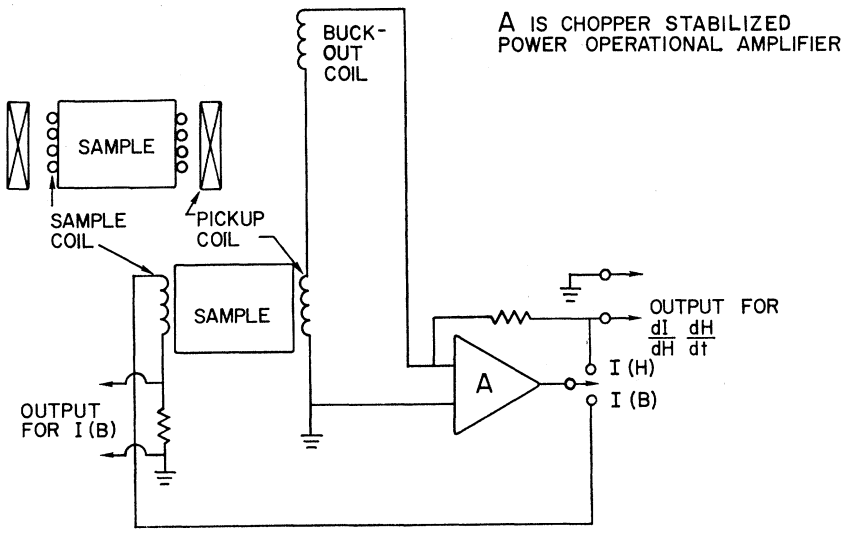

FIG. 2. Experimental arrangement for measurements of I, dI/dH, and dI/dB versus H or B.

i_s, was related to the magnetization intensity I by the simple solenoid formula

$$4\pi I = 4\pi n i_s/10, \tag{15}$$

where n is the number of turns per cm of the sample coil. Thus I versus B is obtained from i_s versus H. The susceptibility dI/dB versus B is obtained by simple RC differentiation.

A second method of measurement is to relate the voltage in the pickup coil to dI/dH directly. For a time varying applied field the voltage in the pickup coil

$$V_p = m\dot{I}_e = \frac{10m}{n}\frac{dI}{dH}\frac{dH}{dt}, \tag{16}$$

where m is the mutual inductance between sample and pickup coils. The quantity m was measured using standard ac techniques at frequencies below the skin depth frequency for our sample. (The quantity m/n can also be obtained for a hypothetical sample coil from standard handbook formulas.) The value $m=5.98\pm0.05$ mH was obtained from these measurements. Using calibrated field sweeps linear in time dI/dH and I (by RC integration) versus H were obtained. The susceptibility dI/dB is obtained from

$$dI/dB = [dH/dI + 4\pi(1-D)]^{-1}, \tag{17}$$

where D is the demagnetizing factor. For our sample shape (see below), we expect $D=\frac{1}{3}$.[23]

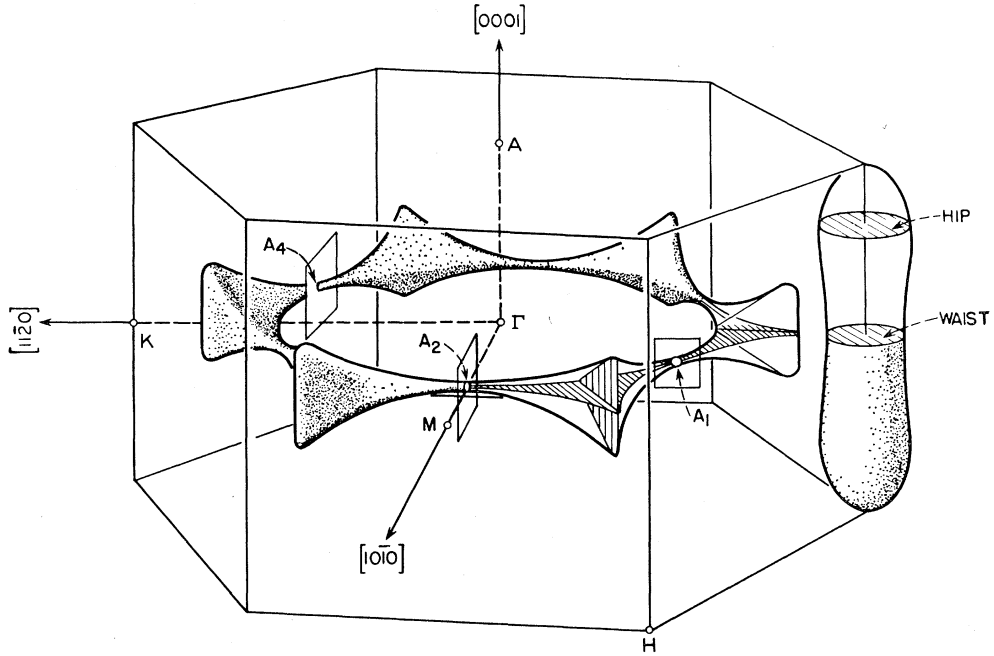

FIG. 3. Fermi surface of Be.

[23] The cubical sample shape will lead to demagnetizing fields which are not uniform throughout the sample volume. Except for $dI/dH \sim -1/4\pi(1-D)$ this contributes a small error.

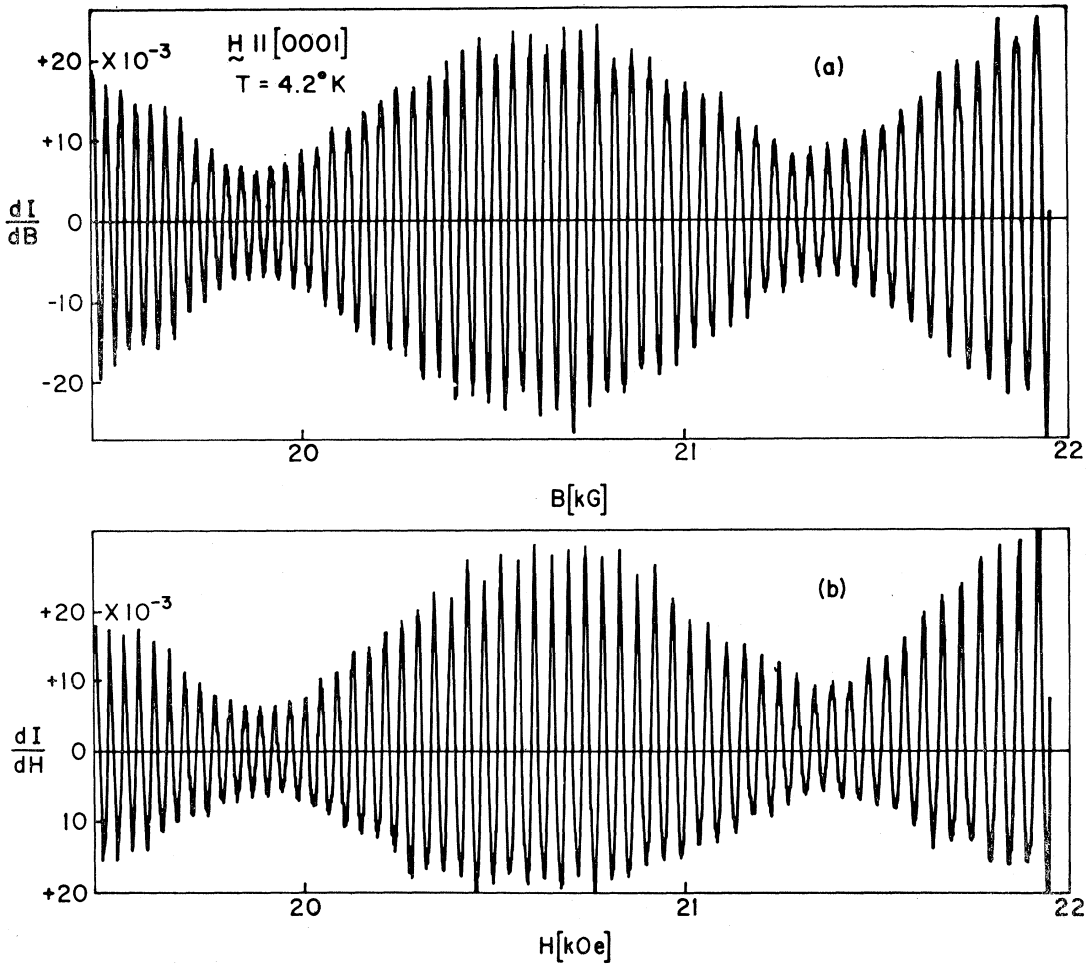

FIG. 4. Magnetic susceptibility oscillations from the "cigars" at 4.2°K with field parallel to [0001]. (a) dI/dB versus B; (b) dI/dH versus H.

The sample coil consisted of 106 turns of No. 40 AWG copper wire tightly wound over the entire length of the sample. The pickup and buckout coils contained about 6000 turns each of No. 46 AWG.

The sample was nearly cubical with approximate dimensions 1.04 cm ($\|[0001]$)$\times$1.1 cm (basal plane directions). The resistance ratio $R(300°\text{K})/R(4.2°\text{K})$ $\approx$2000. This sample was used for all measurements described in this paper.

IV. MAGNETIC SUSCEPTIBILITY RESULTS

The Fermi surface of Be is shown in Fig. 3. The "cigar"-shaped pieces contain electrons and the "coronet"-shaped piece contains an equal number of holes. For magnetic field parallel to the hexagonal axis, the Landau oscillatory effects are dominated by the two extremal cross-sectional areas, "hips" and "waists," which differ by about 3%. For magnetic fields in the basal plane the dominant effect is due to the small "necks" on the coronet.

The experimental results of the dI/dB and dI/dH measurements at 4.2°K with the field along the hexagonal axis are shown in Fig. 4. The asymmetry about the zero line of the dI/dH results is due to the demagnetizing effects. Using $D=\frac{1}{3}$ in Eq. (17), the dI/dB calculated from dI/dH is symmetric and agrees with the direct measurement to 2%. The peak susceptibility dI/dB at the antinode of the two beating frequencies (20.7 kOe) is 23.2×10^{-3} and the mean node to antinode amplitude ratio is 0.28, with the higher frequency which is due to the hips having the larger amplitude. From these data we calculate the following peak susceptibilities:

$$\left.\frac{dI}{dB}\right|_{\text{hips}} = 14.9\times10^{-3}, \qquad 20.7 \text{ kOe}$$

and

$$\left.\frac{dI}{dB}\right|_{\text{waist}} = 8.4\times10^{-3}, \qquad 4.2°\text{K}.$$

The susceptibility data at 1.4°K are shown in Fig. 5. The temperature dependence of the peak paramagnetic and peak diamagnetic susceptibilities are shown in

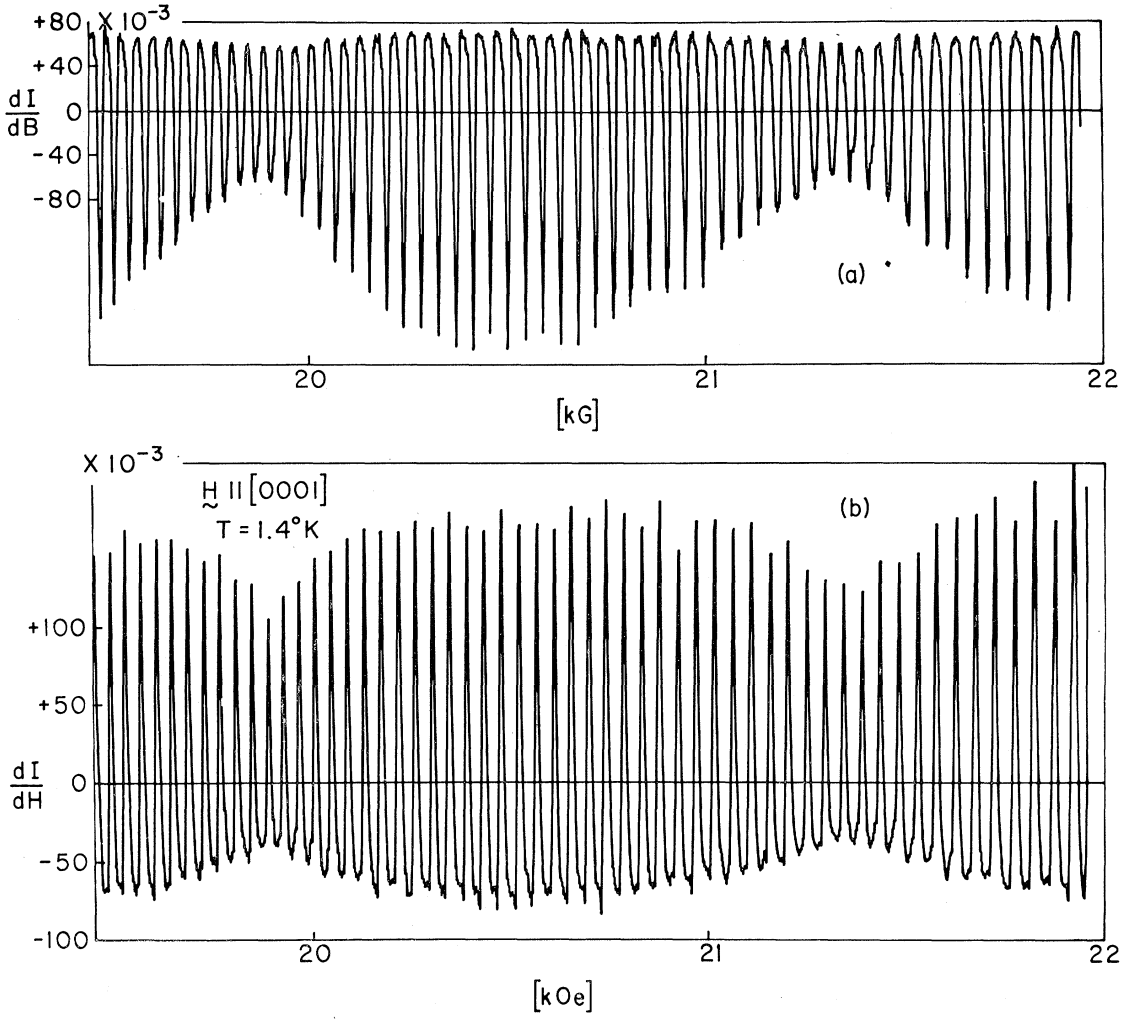

FIG. 5. Magnetic susceptibility oscillations from the "cigars" at 1.4°K with field parallel to [0001]. (a) dI/dB versus B; (b) dI/dH versus H.

Fig. 6. The temperature dependence of the diamagnetic susceptibility can be fit well to the standard theoretical expression by using the value of the cyclotron mass, $m_c=0.17m_0$,[24] determined by Azbel'-Kaner cyclotron resonance. Theoretically the amplitude of the paramagnetic peaks should mirror that of the diamagnetic peaks until it reaches $1/4\pi$, at which value domain formation has been predicted.[12] Below this temperature, no further increase should occur. The data of Fig. 6 tend toward this behavior but do not correspond in detail to it.

Several possible reasons for this discrepancy were considered. At 1.4°K, $d4\pi I/dB(=2.7)$ was sufficiently large, theoretically, for domain formation. The failure of the paramagnetic susceptibility to increase below 2.2°K (while the diamagnetic susceptibility increased by ~45%) also indicates that a sufficiently large susceptibility was obtained. A reduction in susceptibility might occur if crystalline microstructure existed which caused signal dephasing. However, the angular spread in [0001] directions to cause dephasing throughout the paramagnetic phase would be ~7° while backreflection x-ray photographs indicate the true spreading to be ~0.5°. The discrepancy between the observed susceptibility and that predicted for domains formation is not understood.

For $H\|[10\bar{1}0]$, we observe a single period arising from the coronet necks.[25] The susceptibility (see Fig. 7) is weaker than that of the cigar owing largely to the smaller de Haas–van Alphen (dHvA) frequency. A maximum in the susceptibility occurs at 7–8 kOe. Most of the analysis of the sound velocity data was performed in this region to minimize errors due to the suscepti-

[24] W. M. Walsh, Jr. (private communication).

[25] For H in the basal plane the demagnetizing factor corrections in Eq. (17) (which have been applied in the analysis) are generally $\lesssim 5\%$ and $dI/dH \approx dI/dB$.

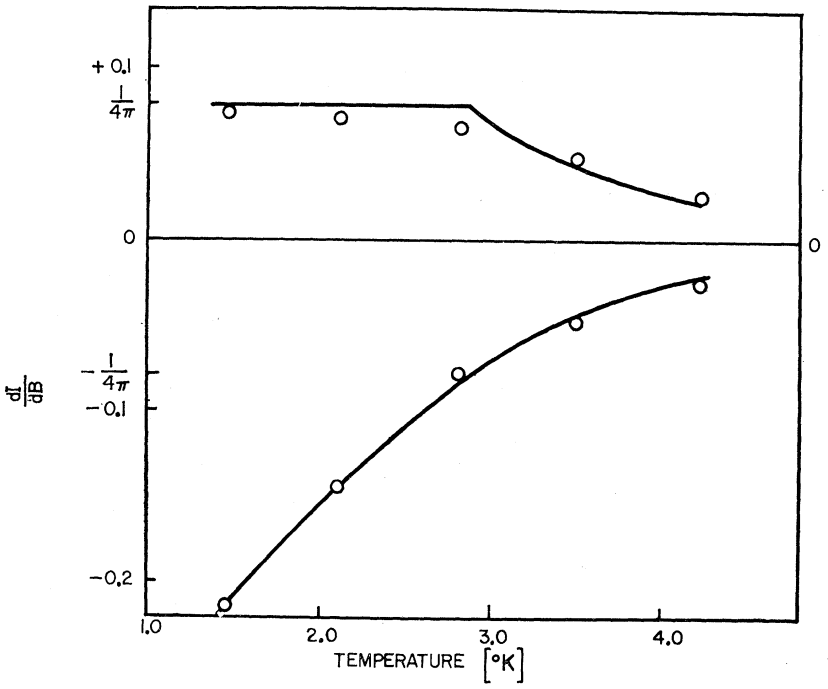

FIG. 6. Temperature dependence of the peak paramagnetic and diamagnetic susceptibilities due to the cigars with $H=20.7$ kOe and $\mathbf{H}\|[0001]$. The solid line is the expected behavior with $m_c=0.17m_0$.

bility measurement. At 4.2°K and 7.45 kOe, dI/dB ($\approx dI/dH^{25}$) $=2.65\times10^{-3}$ (peak-to-peak) and increases by a factor of 2 between 4.2 and 1.4°K. At 1.4°K, dI/dB decreases by a factor of 2.3 from 7.45 kOe to 18.3 kOe. The error in dI/dB is estimated to be $\pm10\%$ at 7.45 kOe.

For $H\|[11\bar{2}0]$, two periods arise from the coronet necks. At 4.2°K we find $dI/dB=1.7\times10^{-3}$ (peak-to-peak) at 5 kOe for the slow period. For the fast period we find $dI/dB=1.9\times10^{-3}$ (peak to peak) at 10 kOe and 1.4°K. Errors are generally $\pm10\%$.

V. EXPERIMENTAL METHOD FOR VELOCITY MEASUREMENT

The basic method used for the sound velocity measurements was the McSkimin pulse superposition method.[13] In this method, shown schematically in Fig. 8, the sound is resonantly excited at a period which is

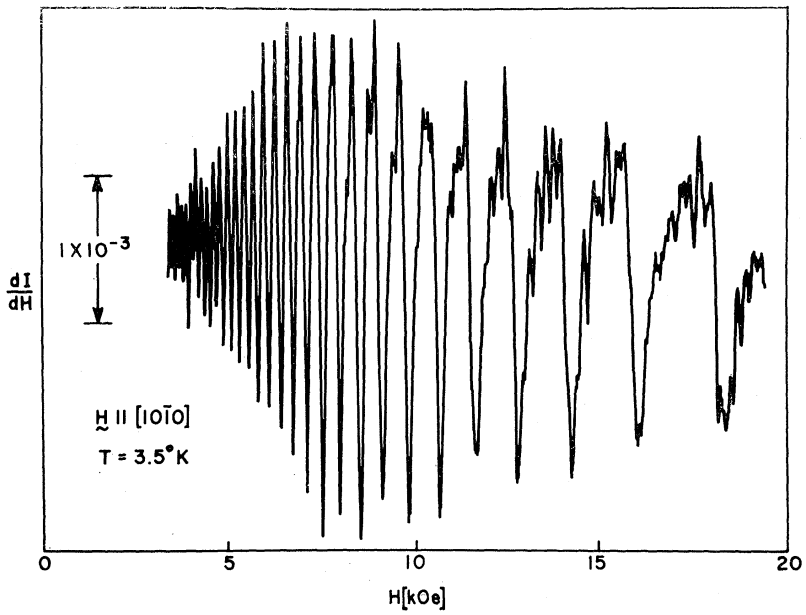

FIG. 7. dI/dH versus H for $\mathbf{H}\|[10\bar{1}0]$. The oscillations arise from the "coronet" necks.

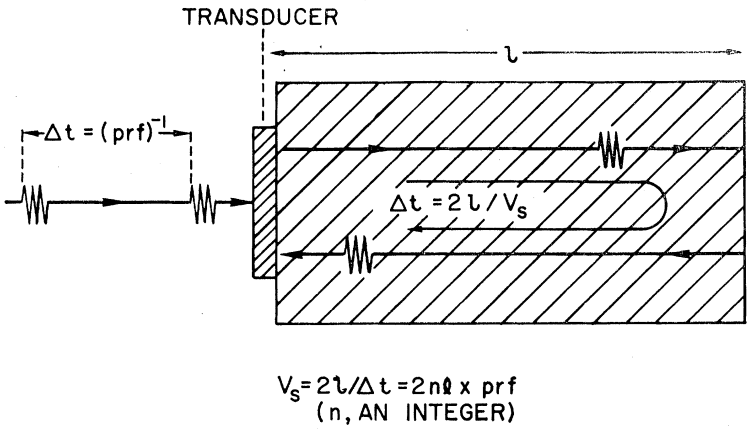

FIG. 8. Schematic representation of McSkimin pulse superposition method for sound velocity measurement.

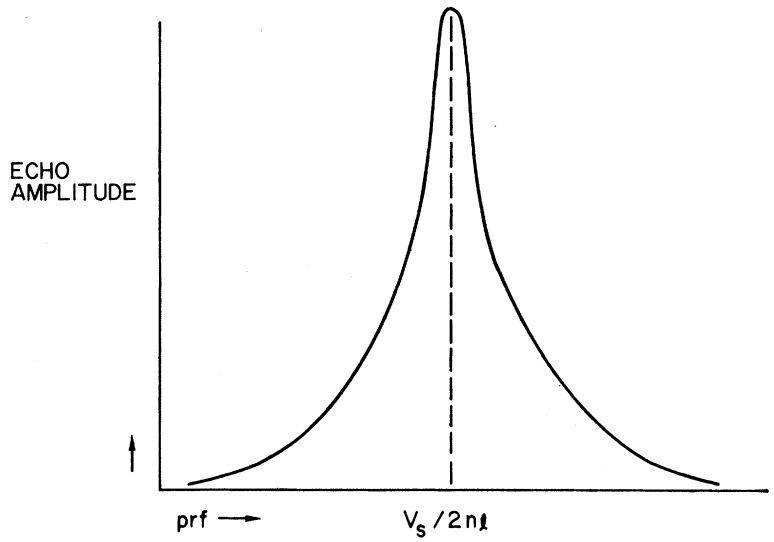

twice[26] the round trip time of sound in the sample. For pulse repetition frequencies (PRF) near resonance the amplitude of the arriving echoes as a function of the PRF is shown in Fig. 8. The PRF at peak response gives the sound velocity.

We have modified the McSkimin technique by using FM and AFC techniques to lock on resonance and to allow continuous calibrated recording of high precision. A block diagram of the arrangement is shown in Fig. 9. The pulse repetition rate is derived from a General Radio synthesizer which is frequency modulated at 500 Hz. The synthesizer output (normally in the 30–60-MHz range) was scaled[27] by 200 before triggering a pulsed 20-MHz oscillator. Quartz or tourmaline transducers were used to generate the sound. The 20-MHz echo signals were converted for amplification and video detection in a 30-MHz i.f. strip. Although the recovery time of the i.f. strip after r.f. pulsing is sufficiently fast for easy detection of echoes, the high PRF's of this technique cause the gain to vary with the PRF. To avoid gain modulation at the frequency of modulation the driving pulses were blocked from the i.f. strip by switching off the local oscillator (LO) during the driving time. A separate pulser triggered by the prf signal was used to open the solid state switch linking the LO and mixer. An *RC* filter rejects the high-frequency components of the video signal and the 500-Hz amplitude modulation is phase detected by Princeton Applied Research Corporation HR-8 (PAR). The dc output (control) signal is reduced by a simple divider[28] and fed to the frequency sweep input of the synthesizer.

Continuous recording of the resonant PRF was performed using the "beat" frequency output of the

[26] Integer multiples other than two may be used.

[27] The phase stability of the synthesizer is increased by using the higher frequencies and scaling.

[28] The divider is used to increase the PAR control signal well beyond the no signal noise level in the dc stage. A 1-kHz twin tee filter was also used at the PAR input to prevent overload from the FM second harmonic.

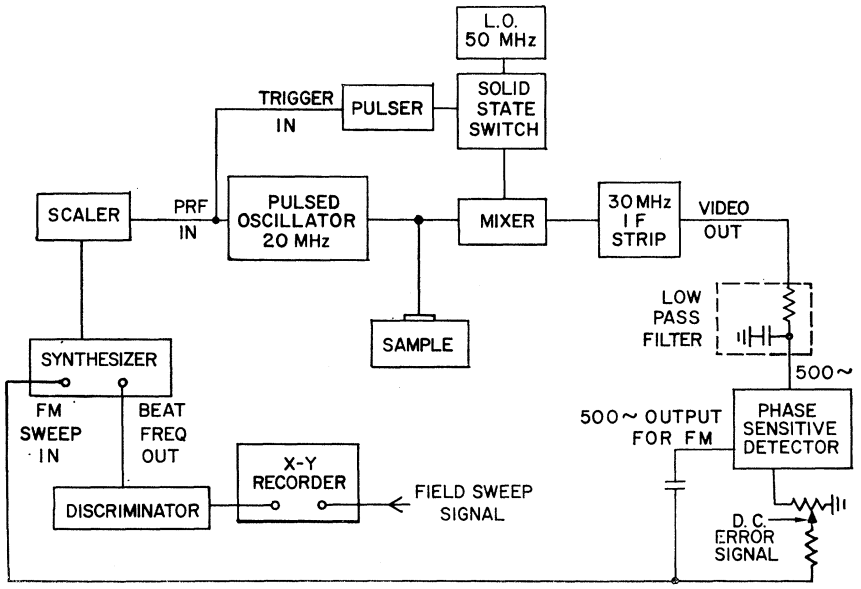

FIG. 9. Block diagram of system for measuring sound velocity.

synthesizer. This output frequency is proportional to that of the frequency swept decade (usually the fourth) only. An analog voltage for recording is obtained using a General Radio 1142-A frequency meter and discriminator. The 500-Hz FM signal is capacitor filtered at the output.

With sufficient gain in the PAR the system "locks in" on the PRF for peak response. Loop gain was generally greater than 200. The PAR time constant was normally 10 sec and 6 dB/octave. With this loop gain the response time was less than 50 msec. The sensitivity and stability of this system depend on the attenuation of sound in the sample and the quality of the acoustic bond between the transducer and sample. The sensitivity to small changes was generally 2×10^{-7} to 2×10^{-8}. For large changes (up to one part in 10^{-3}) the control and recording system was accurate to $\sim0.3\%$.

The response of the AFC system to attenuation changes is ideally zero. In practice, i.f. gain changes of a factor of 2 (6 dB) caused shifts of $\lesssim10^{-6}$ in the PRF. The Landau quantum oscillations in attenuation which occurred during measurement were smaller than this by 2–3 orders of magnitude.

VI. SOUND VELOCITY RESULTS

A. Elastic Moduli at Zero Field

The five independent nonvanishing components of the (hexagonal) Be elastic modulus tensor are

$$c_{11}=c_{22}, \qquad c_{44}=c_{55},$$
$$c_{13}=c_{31}=c_{23}=c_{32}, \qquad c_{66}=\tfrac{1}{2}(c_{11}-c_{12}),$$
$$c_{33}$$

A simple array which associates strains and elastic moduli with propagation directions and particle motions used in this experiment is shown in Table I. The diagonal components of this array are obtained with longitudinal waves and the off-diagonal components are obtained with shear waves. Because of symmetry relations, only four of the five independent elastic modulus tensor components are obtained from shear and longitudinal waves propagating in the high-symmetry directions. The sixth component, c_{13}, which must be obtained from an "off-axis" wave, has not been studied in our work. Furthermore, no propagation along $[11\bar{2}0]$ was made. The sound velocities and elastic moduli obtained at 4.2°K in zero field are shown in Table II. In calculating the elastic moduli we have used the room-temperature x-ray density[29] 1.8477 g/cm³. Thermal contraction corrections ($\sim10^{-3}$) has been estimated from the work of Erfling.[30] The estimated accuracy in c and V_s is 0.1%. With the exception of c_{11} (and, accordingly, c_{12}) these elastic moduli agree with those reported by Smith and Arbogast[31] to within $\sim0.5\%$ which is the combined estimated error. Although our sample was no doubt considerably purer than theirs, the difference in c_{11} is larger than what one normally expects for small impurity effects. Table II also gives the components of

TABLE I. Strains and elastic moduli for high-symmetry sound modes.

Particle motion	Propagation direction $[10\bar{1}0]$	$[11\bar{2}0]$	$[0001]$
$[10\bar{1}0]$	$\epsilon_1; c_{11}$	$\epsilon_6; c_{66}$	$\epsilon_5; c_{55}$
$[11\bar{2}0]$	$\epsilon_6; c_{66}$	$\epsilon_2; c_{22}$	$\epsilon_4; c_{44}$
$[0001]$	$\epsilon_5; c_{55}$	$\epsilon_4; c_{44}$	$\epsilon_3; c_{33}$

[29] J. T. Stacy, U. S. Atomic Energy Commission Report No. AECD-3647, 1955 (unpublished).
[30] H. D. Erfling, Ann. Physik **34**, 136 (1939).
[31] J. F. Smith and C. L. Arbogast, J. Appl. Phys. **31**, 99 (1960).

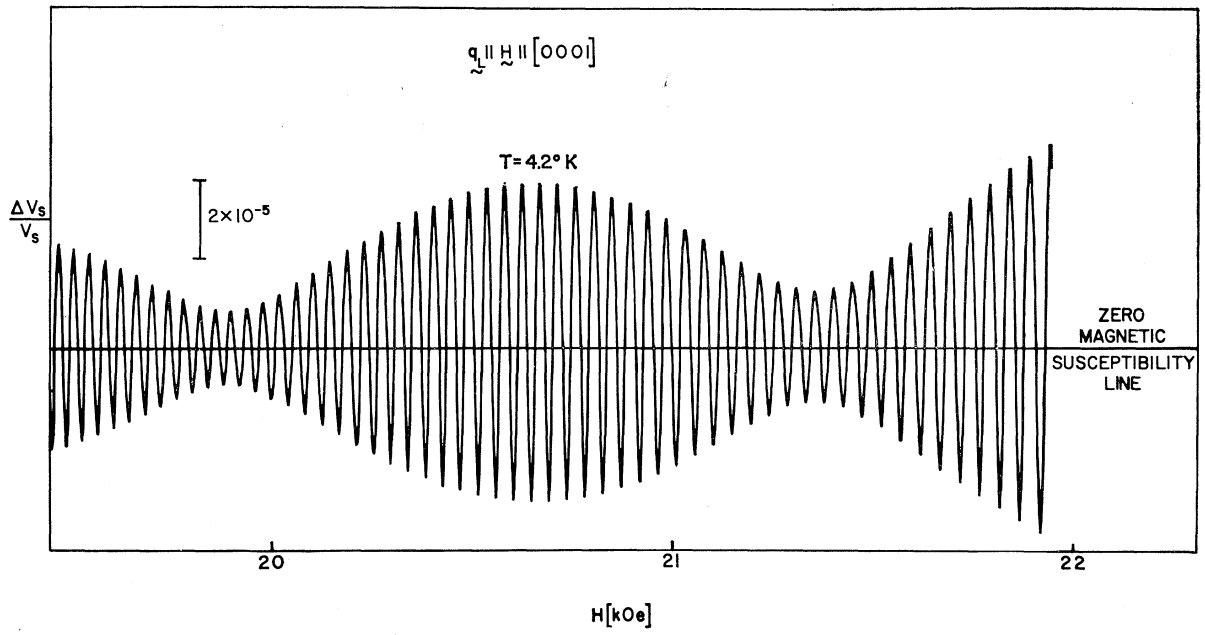

FIG. 10. Sound velocity oscillations due to the cigars. $q_L \| \mathbf{H} \| [0001]$, $T=4.2$°K.

the compliance tensor. In inverting our c tensor, we have used the c_{13} of Smith and Arbogast.

B. Landau Quantum Oscillations

$\mathbf{H} \| [0001]$ ("*Cigars*")

For longitudinal waves propagating along [0001] (ϵ_3 strains) the oscillations at 4.2°K (see Fig. 10) are found to be symmetrical about the zero line in agreement with dI/dB (and not dI/dH). The mean node-to-antinode ratio at 20.7 kG is 0.285 (hip frequency dominant) which is very nearly that value (0.28) obtained for the dI/dB results. The deformation parameters $D_i \equiv d \ln A/d\epsilon_i$ obtained from these results are given in Table III. The algebraic signs have been inferred from the magnetostriction results of Chandrasekar, Fawcett, Sparlin, and White[32] (CFSW).

TABLE II. Elastic moduli of Be at 4.2°K.

	Stiffness moduli	
	Present work	Smith and Arbogast[a]
	Units (10^{11} dyn/cm^2)	
c_{11}	28.58	29.94
c_{33}	34.28	34.22
c_{44}	16.69	16.62
c_{66}	13.52	13.59
c_{12}	1.48	2.76
c_{13}	···	1.1
	Compliance moduli[b]	
	Units (10^{-14} cm^2/dyn)	
s_{11}	35.12	33.72
s_{33}	29.24	29.29
s_{44}	59.92	60.17
s_{66}	73.96	73.58
s_{12}	−1.78	−3.07
s_{13}	−1.07	−0.099

[a] Reference 31.
[b] Our compliance moduli have been obtained using c_{13} of Smith and Arbogast (Ref. 31).

TABLE III. Deformation parameters for Be Fermi surface.[a]

	Cigars ($\mathbf{H} \| [0001]$)				
	Present work		Magneto-striction results[b]	Calculated results[c]	
	Hip	Waist		Hip	Waist
D_1	+1.86	+2.30	+1	+0.68	+1.14
D_2	(+1.86)	(+2.30)	+1	+0.68	+1.14
D_3	−5.3	−5.28	−6	−2.2	−2.1
D_4	∼0	∼0			
D_5	∼0	∼0			
D_6	∼0	∼0			

	Coronet necks					
	A_2 (Minimum cross section)		A_1 (30° from A_2)		A_4 (60° from A_2)	
	Present work	Magneto-striction results[b]	Present work	Magneto-striction results[b]	Present work	Magneto-striction results[b]
D_1	−60	−50	+88	+70	···	···
D_2	···	+150	···	−8	···	···
D_3	−63	−50	−65	−50	−63	···
D_4	0	···	0	···	0	···
D_5	0	···	0	···	0	···
D_6	0	···	±90	···	±81	···

[a] $D_i = d \ln A/d\epsilon_i$. The error is ±10% for our results and ±20% for those of CFSW. For our results we have assumed $D_1 = D_2$ for the cigars.
[b] The magnetostriction results are from CFSW, Ref. 32. The hip and waist parameters were not distinguished in these results.
[c] Calculated results from Tripp *et al.*, Ref. 36.

[32] B. S. Chandrasekar, E. Fawcett, D. M. Sparlin, and G. K. White, in *Proceedings of the Tenth International Conference on Low Temperature Physics* (VINITI, Moscow, 1967), Vol. 3, p. 328.

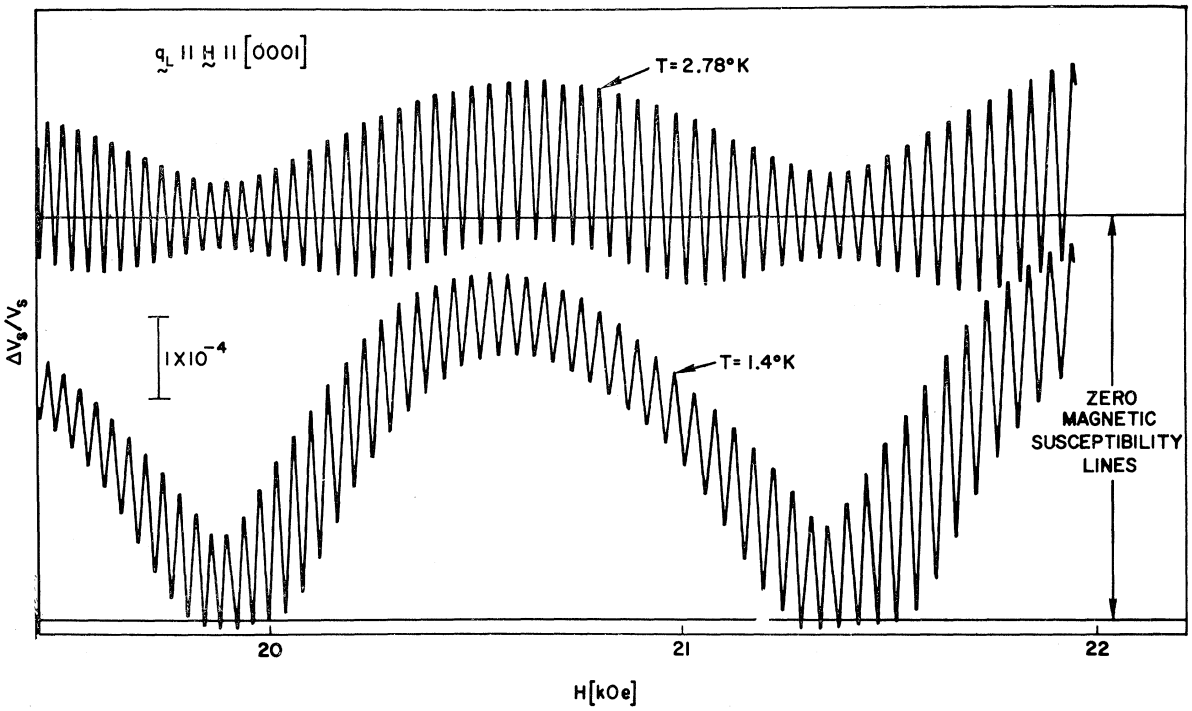

FIG. 11. Sound velocity oscillations due to cigars. $\mathbf{q}_L \| \mathbf{H} \| [0001]$, $T=2.78°K$ (upper) and 1.4°K (lower). Envelope distortion results from magnetic interactions. The zero magnetic susceptibility line for the 1.4°K data was extrapolated from lower fields where the wave shape distortion is small.

For longitudinal waves propagating along $[10\bar{1}0]$ at 4.2°K the softening (paramagnetic) peaks are smaller than the stiffening (diamagnetic) peaks. This asymmetry has the form expected for MI effects but no such asymmetry is found in the dI/dB susceptibility data at 4.2°K. Although the cause of this behavior is not known we have chosen the stiffening (diamagnetic) peaks of the sound velocity oscillations for analysis. This choice leads to deformation parameters which are only 7% greater than those obtained from the peak-to-peak magnitude of the oscillations. At 20.7 kOe, the mean node-to-antinode ratio is 0.18 (hip frequency dominant). The deformation parameters obtained from these data are given in Table III. From CSFW[32] we have taken the algebraic sign to be positive. It is seen that the Alpher-Rubin term [see Eq. (11)] which appears in this case, contributes ~30% of the amplitude of the oscillations.

For all three transverse waves propagated in this experiment the amplitudes of the oscillations were roughly two orders of magnitude smaller than those obtained with the longitudinal waves. Ideally one expects a null effect in this case because the shear deformation parameters and (for $\mathbf{q}_T \| [0001]$) the oscillatory Alpher-Rubin contribution vanish by symmetry. The weak oscillations which were observed depended in amplitude largely upon the quality of the transducer-sample bond. For bonds which gave the best exponential echo decay the oscillations were smallest. These oscillations may result from extraneous sound modes in the sample. Their amplitudes would be equivalent to D's$\lesssim 0.2$.

Low Temperatures and Effect of Magnetic Domains

Below approximately 3.2°K a severe distortion of the beat envelope appears during the softening phase. The results for $\mathbf{q}_L \| [0001]$ at $T=2.78°K$ are shown in Fig. 11. A similar envelope distortion occurs for $\mathbf{q}_L \| [10\bar{1}0]$. The onset of these distortions coincides, approximately, with $d4\pi I/dB=1$. In Fig. 12 we show the temperature dependence of the amplitude of the sound velocity oscillations ($\mathbf{q}_L \| [0001]$) for the softening and stiffening peaks. As T is lowered the stiffening amplitude of the oscillations (at the antinode) continues to increase while the softening amplitude decreases. At 1.4°K (Fig. 11) the distortion has given rise to a separate large difference frequency.[33] The base line for the sound velocity oscillations is taken at the midpoint of the oscillations at the nodes where the MI effect is relatively small.[34] Since the sound velocity should be proportional to dI/dB even in the domain state the results at 1.4°K

[33] B. B. Chick, G. P. Anderson, and R. Truell have recently observed the difference frequency (only) in this field range (private communication).

[34] In fact, at $T=1.4°K$, $d4\pi I/dB \sim 1$ at the nodes for $H \sim 20$ kOe and this choice of baseline will be in error. One can establish the proper baseline, however, by examining the data at lower fields where $d4\pi I/dB < 1$ at the nodes.

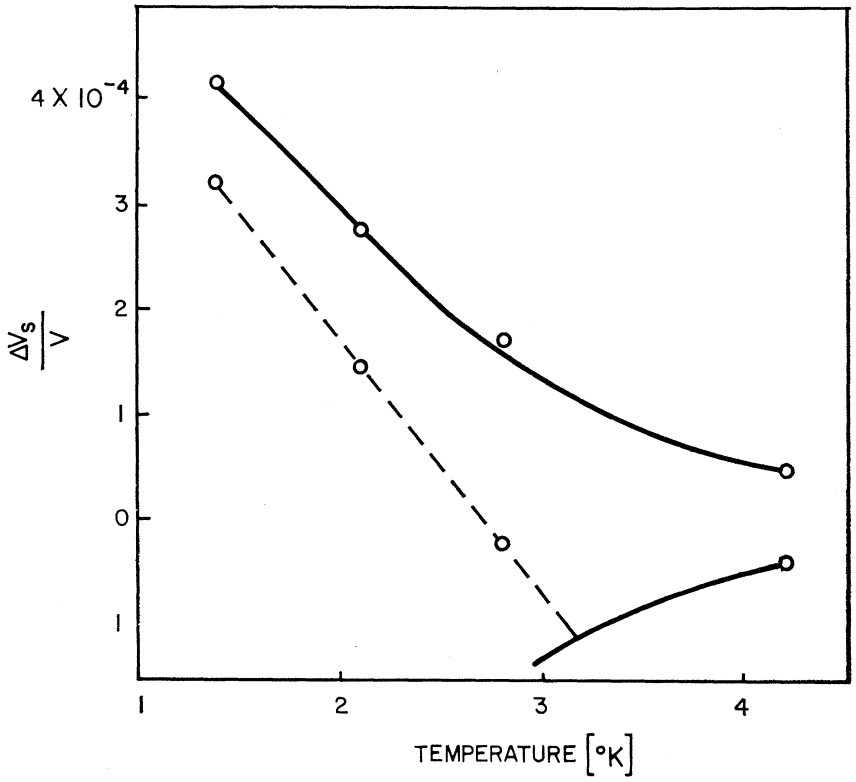

FIG. 12. Temperature dependence of the peak sound velocity deviations due to the cigars for $H=20.7$ kOe and $\mathbf{H}\|\mathbf{q}_L\|[0001]$. The solid line is the calculated behavior for no domains. The data below 3° agree qualitatively with the model of no domain wall motion at 20 MHz. A line connecting data points has been included for clarity.

show that the sample does not exhibit paramagnetism (except near the nodes) at the sound wave frequency (20 MHz). This behavior is in agreement with that expected for domains whose walls are immobile at the 20-MHz sound frequency (see Sec. II).

For the diamagnetic susceptibility, no anomalies are expected and it is a satisfying check on the theory that between 4.2 and 1.4°K at $H=20.7$ kOe the magnitude of the stiffening peaks increases by a factor of 9.5 while the predicted increase (from dI/dB) is 9.3.

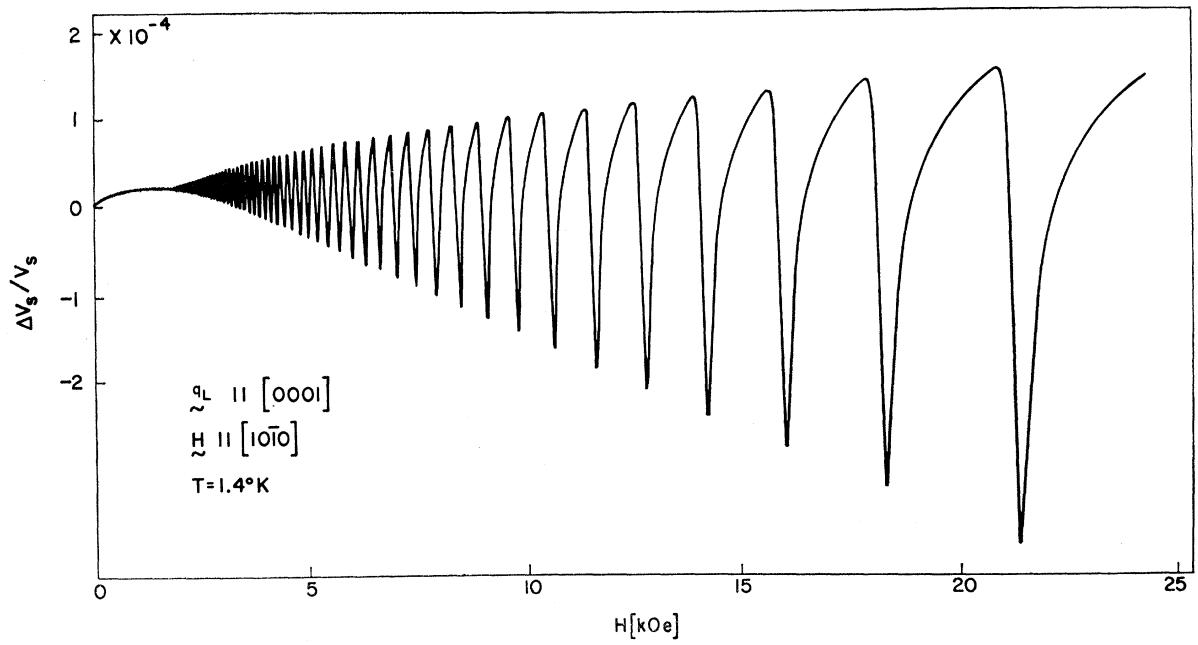

FIG. 13. Sound velocity oscillations due to coronet necks. $\mathbf{q}_L\|[0001]$, $\mathbf{H}\|[10\bar{1}0]$, $T=1.4$°K.

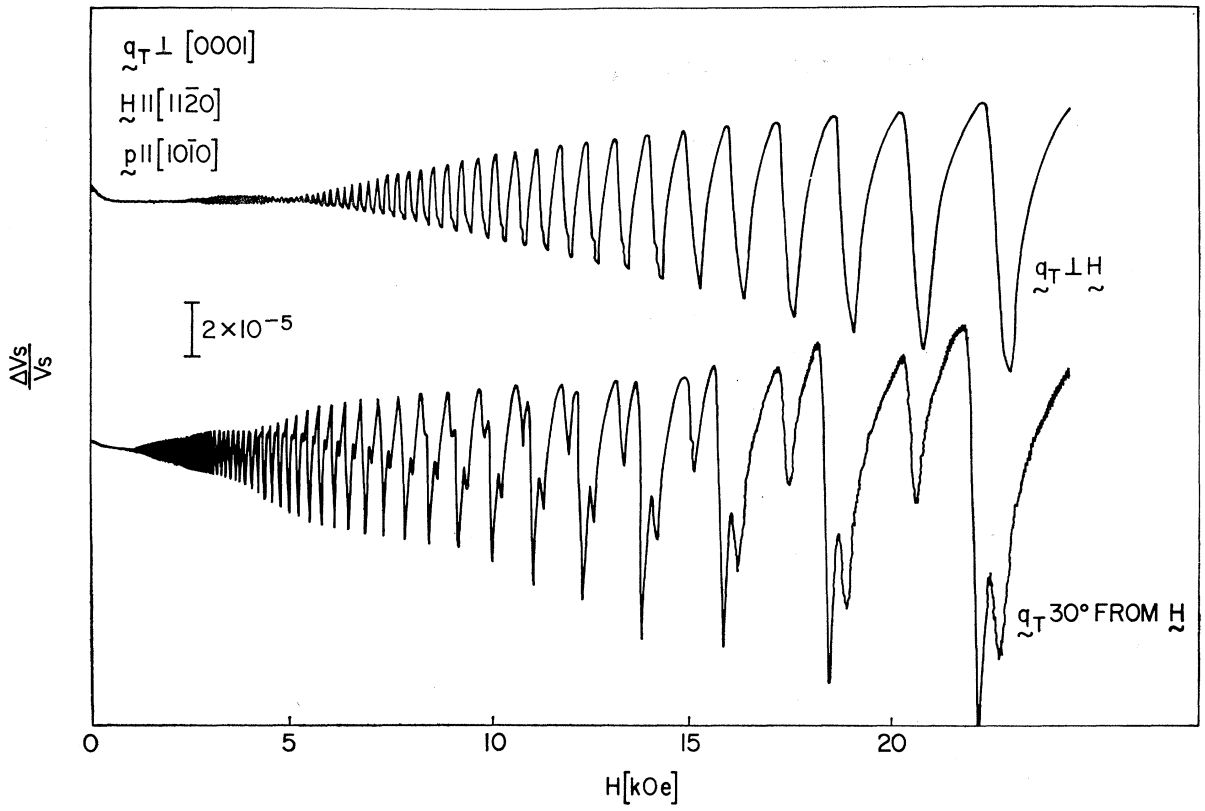

FIG. 14. Sound velocity oscillations due to coronet necks. $\mathbf{q}_T \| [10\bar{1}0]$, $\mathbf{p} \| [11\bar{2}0]$, $\mathbf{H} \| \langle 11\bar{2}0 \rangle$. Upper, $\mathbf{H} \perp \mathbf{q}_T$; lower, $\mathbf{H}$ in basal plane but 30° from $\mathbf{q}_T$. (Splittings may be due to slight misorientation.)

$\mathbf{H} \| [10\bar{1}0]$ ("*Coronet*" *Necks*)

For $\mathbf{H}$ in this direction a single Landau quantum period is obtained from the coronet necks. The results for $\mathbf{q}_L \| [0001]$ at 1.4°K are shown in Fig. 13. The softening spikes at the highest fields and lowest temperatures allow a test of Eq. (12) for oscillations with large harmonic content. For all sound waves propagated with this field direction Eq. (12) was verified to within $\pm 10\%$ for all fields (>5 kOe) and temperatures.

For this field direction the shear component of the deformation parameter need not be zero. Indeed the largest oscillations observed in our experiments were obtained with $\mathbf{q}_T \| [10\bar{1}0]$ and $\mathbf{p} \| [11\bar{2}0]$. At 1.4°K and 18.3 kOe the softening peaks in velocity were $\sim 0.25\%$.

An interesting example of how the hexagonal symmetry is broken by the sound deformation occurs for the case $\mathbf{q}_T \| [1010]$, $\mathbf{p} \| [11\bar{2}0]$. For $\mathbf{q}_T \cdot \mathbf{H} = 0$ the four coronet necks are equivalent in area as well as strain dependence (see Fig. 3). For $\mathbf{H}$ rotated by 60° two of the extremal areas are strain independent (by symmetry). For this configuration we find the oscillation amplitude to be just one-half that obtained with $\mathbf{q}_T \cdot \mathbf{H} = 0$.

The deformation parameters obtained for the five different modes are given in Table III. The algebraic signs are taken from CFSW.[32] The oscillatory Alpher-Rubin contribution to D for the shear wave results [see Eq. (12)] is $\sim 1\%$ and has been ignored.

$\mathbf{H} \| [11\bar{2}0]$ ("*Coronet*" *Necks*)

With H parallel to $[11\bar{2}0]$ two Landau quantum periods may result from the coronet necks. These correspond to the minimum coronet neck area A_2 and that neck area obtained by a 60° rotation A_4. Although both periods occur in the magnetization, one of these may be absent from the sound velocity results because of (sound) broken hexagonal symmetry.

For the oscillations obtained with $\mathbf{q}_L \| [0001]$ both periods occur with relative magnitudes similar to those found in dI/dB. The deformation parameters are therefore equal for the two extremal areas, a behavior expected for cylindrical arms of the coronet under ϵ_3 strain.

The reduction of symmetry introduced by the sound wave can be seen for the case of the shear wave $\mathbf{q}_T \| [10\bar{1}0]$, $\mathbf{p} \| [11\bar{2}0]$ with $\mathbf{q}_T \cdot \mathbf{H} = 0$. This shear should not change the smaller area and no corresponding sound velocity oscillations should occur. The oscillations arise only from the four equivalent larger areas. If the field is rotated 60° in the (hexagonal) basal plane ($\mathbf{q}_T \cdot \mathbf{H} \neq 0$) the smallest area is now shear-dependent and the low-

TABLE IV. Hydrostatic pressure derivatives of the "cigar" extremal area (units of 10^{-13} cm^2/dyn $=10^{-4}$ kbar^{-1}).

	Present work	Magneto-striction results[a]	Direct measure-ment[b]	Calcu-lated[c]
$d\ln A_h/dP$	$+2.5(\pm2)$	$+10(\pm4)$	$+2(\pm0.5)$	$+1.7$ ±1
$d\ln A_w/dP$	$-0.7(\pm2)$	$+10(\pm4)$	$-0.8(\pm0.5)$	-1.9 ±1

[a] From CFSW, Ref. 32.
[b] From O'Sullivan and Shirber, Ref. 35.
[c] From Tripp *et al.*, Ref. 36.

frequency oscillation will appear. Furthermore, of the extremal areas giving the high frequency only two are now shear-dependent. Both the appearance of the low-frequency oscillations and the amplitude reduction of the high-frequency oscillations are confirmed in the results (Fig. 14).

For all other shear waves, symmetry arguments require a null effect. The observed oscillations were about three orders of magnitude smaller than those discussed above. The components of the deformation tensor for the two extremal areas obtained with $\mathbf{H}\|[11\bar{2}0]$ are given in Table III.

For several field and sound orientations data were also taken at 60 and 100 MHz. The results were found to be independent of frequency to within 10%, the estimated error for this test. Also, for several orientations, the Landau quantum oscillations of the sound attenuation ($\sim10^{-2}$ to 10^{-3} dB/cm at 20 MHz) were also recorded. The attenuation α maxima generally coincided with the velocity minima, a result expected for a simple general loss mechanism where α is proportional to V_s^{-3}.

VII. COMPARISON WITH EXISTING DATA

The strain dependence of the Be Fermi surface has been obtained by magnetostriction studies[32] and directly from the change in dHvA frequencies under hydrostatic pressure.[35] In the former case the deformation parameters for each of the longitudinal strains ($\epsilon_1,\epsilon_2,\epsilon_3$) have been obtained. The results are given in Table III. For the cigars the waist and hip extremal areas are not distinguished. The largest discrepancy with our results occurs for $d\ln A/d\epsilon_1$ in which our mean value (for waist and hip) is about twice that obtained from the magnetostriction results. Since the ratio $(d\ln A/d\epsilon_1)/(d\ln A/d\epsilon_3)$ (which is independent of dI/dB) is also in error by about a factor of 2 this discrepancy probably does not result from errors in the magnetic susceptibility measurement.

O'Sullivan and Schirber[35] have measured the change in Fermi-surface extremal areas of Be under hydrostatic pressure. The change in extremal area, A, for a stress σ can be calculated from the components of the deformation tensor D by

$$d\ln A=\mathbf{D}\cdot\mathbf{S}\cdot\boldsymbol{\sigma},$$

where $\mathbf{D}$ and $\boldsymbol{\sigma}$ are 1×6 and 6×1 matrices and S is the 6×6 compliance matrix for the material. For hydrostatic pressure $\sigma_1=\sigma_2=\sigma_3=-P$ and $\sigma_4=\sigma_5=\sigma_6=0$. The calculated and observed pressure derivatives of the cigars are given in Table IV. The hydrostatic pressure derivatives are an order of magnitude smaller than the uniaxial stress terms because of a near cancellation of the contribution from the three components of the stress tensor. The errors in the calculated values are, accordingly, quite large fractionally. These calculated values do agree with the observed result considerably better than those calculated from the magnetostriction results.

For the coronet necks the agreement between sound velocity and magnetostriction results is reasonably good. The discrepancy is systematic and probably arises from errors in dI/dB. Since ϵ_2 strain derivatives were not obtained in our experiments we cannot calculate the pressure derivatives. To obtain agreement for $d\ln A_2/dP(=-40\times10^{-13}$ cm^2/dyn from Ref. 35) we require $d\ln A_2/d\epsilon_2\approx125$ which is in reasonable agreement with the magnetostriction result of 150.

Also given in Tables III and IV are the strain dependences of the Be Fermi surface recently calculated by Tripp.[36]

ACKNOWLEDGMENTS

The authors express their gratitude to W. Royer and J. Wellendorf for technical assistance.

[35] W. J. O'Sullivan and J. E. Schirber, Phys. Letters **25A**, 124 (1967); J. E. Shirber and W. J. O'Sullivan, Phys. Rev. **184**, 628 (1969).

[36] R. W. Tripp, P. M. Everett, W. L. Gordon, and R. W. Stark, Phys. Rev. **180**, 669 (1969).